Article

A Functionally and Anatomically Bipartite Vocal Pattern Generator in the Rat Brain Stem

bipartite vocal pattern generator

PAG

VoPaRt:
frequency modulation
high frequency calls

NRA:
pure tones
low frequency calls

Konstantin Hartmann,
Michael Brecht

michael.brecht@bccn-berlin.de

HIGHLIGHTS
Cooling and stimulation reveal two brainstem regions involved in vocal patterning

Both regions consist of very small cells and are highly myelinated

The anterior region (VoPaRt) controls frequency-modulated, high-frequency calls

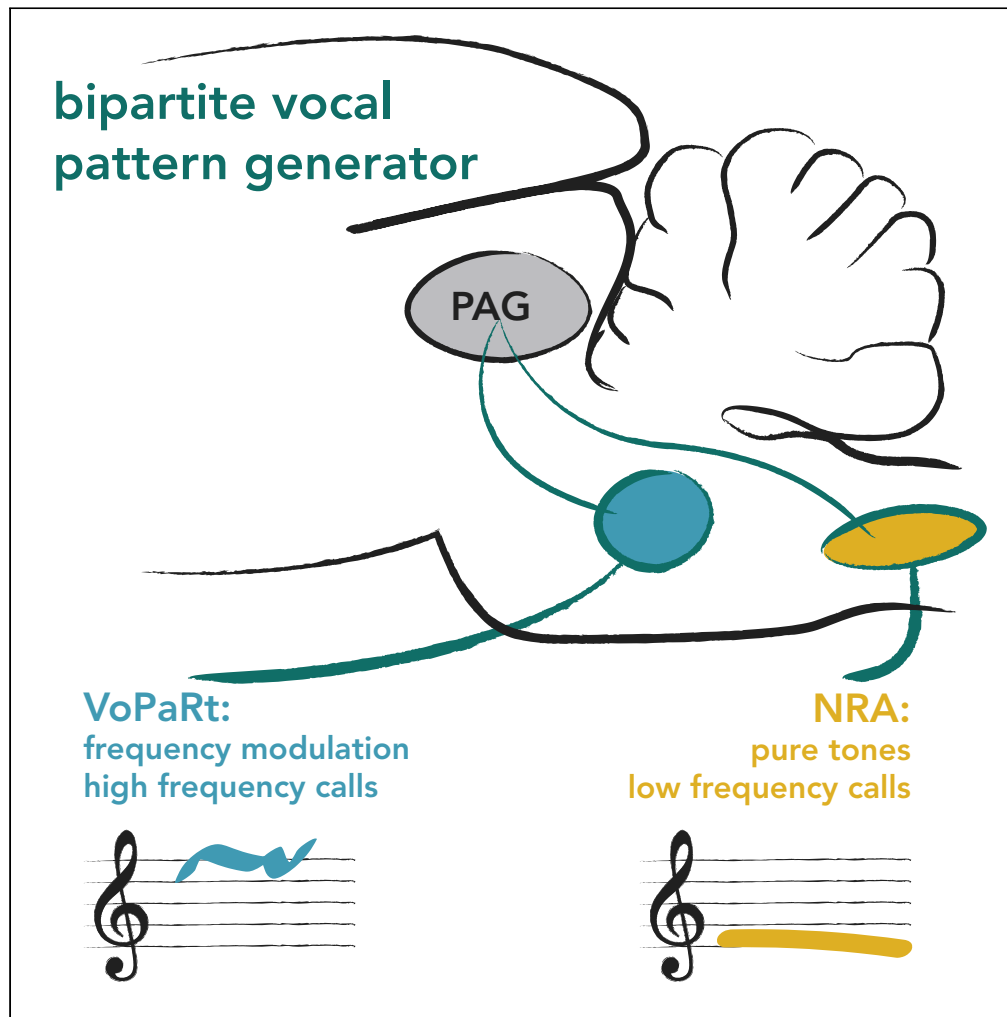The posterior region (NRA) mostly controls flat, low-frequency calls

iScience

Article

A Functionally and Anatomically Bipartite Vocal Pattern Generator in the Rat Brain Stem

Konstantin Hartmann[1] and Michael Brecht[1,*]

SUMMARY

The mammalian vocal pattern generator is situated in the brainstem but its exact structure is debated. We mapped these circuits in rats by cooling and microstimulation. Local cooling disrupted call production above an anterior and a posterior brainstem position. Anterior cooling affected predominantly high-frequency calls, whereas posterior cooling affected low-frequency calls. Electrical microstimulation of the anterior part led to modulated high-frequency calls, whereas microstimulation of the posterior part led to flat, low-frequency calls. At intermediate positions cooling did not affect calls and stimulation did not elicit calls. The anterior region corresponds to a subsection of the parvicellular reticular formation that we term the vocalization parvicellular reticular formation (VoPaRt). The posterior vocalization sites coincide with the nucleus retroambiguus (NRA). VoPaRt and NRA neurons were very small and the VoPaRt was highly myelinated, suggestive of high-speed processing. Our data suggest an anatomically and functionally bipartite vocal pattern generator.

INTRODUCTION

Vocalizations arise from some of the most complex motor patterns produced by vertebrates. The sheer complexity of the vocalization process makes understanding its neural underpinnings very challenging. It is therefore not surprising that a great number of brain structures are involved in vocalization control. The role of the forebrain in vocalizations has been highlighted early by Broca's discovery (Broca, 1861) of left hemispheric speech localization, and numerous studies on songbirds have clarified the role of avian forebrain circuits in song learning (Sakata et al., 2020). Downstream of the forebrain, an important structure for vocalizations is the periaqueductal gray (PAG). Its involvement in vocalizations is long known (Jürgens, 1994), and a recent study manipulated neuronal firing in the PAG evoking or inhibiting vocalizations, underlining its gateway functions for call production (Tschida et al., 2019). In mammals, there is also a consensus that brainstem circuits coordinate the patterning of vocalizations. This conclusion rests on the following observations: (1) Electrical (Bennett et al., 2019; Jürgens and Ploog, 1970; Kyuhou and Gemba, 1998) and chemical (Lu and Jürgens, 1993; Zhang et al., 1995) stimulation of forebrain and midbrain circuits upstream of the brainstem often evokes species-specific, complex, and complete vocalizations; (2) electrical (Dressnandt and Jürgens, 1992) and chemical (Jürgens and Richter, 1986) stimulation of brainstem sites often evokes artificial and elementary vocalizations; (3) several different structures in the brainstem project to all involved phonatory motor neuron pools (Fay and Norgren, 1997; Hannig and Jürgens, 2005; Thoms and Jürgens, 1987).

These observations have led to the idea of a vocal patterning generator localized in the brainstem, but there is no clear picture yet of the identity of the putative vocal pattern generator (VPG), especially in the rodent. In fact, as shown in Figure 1A, there are competing accounts of the mammalian VPG. Based on anatomical evidence from the cat, Holstege (1989) suggested that the VPG is situated in the nucleus retroambiguus (NRA, Figure 1A, left). In line with this idea, lesions and transections of the NRA result in an abolishment of calls (Holstege, 1989; Zhang et al., 1995) and the NRA projects to the relevant motor neuron pools. Competing with this model is the suggestion that the VPG is widely spread through the reticular formation (Figure 1A right) (Jürgens and Hage, 2007; Lüthe et al., 2000). Neuronal activity close to the superior olive in squirrel monkeys correlated with vocalizations, especially frequency modulated ones (Hage and Jürgens, 2006a, 2006b). Although neuronal recording data contribute important correlative
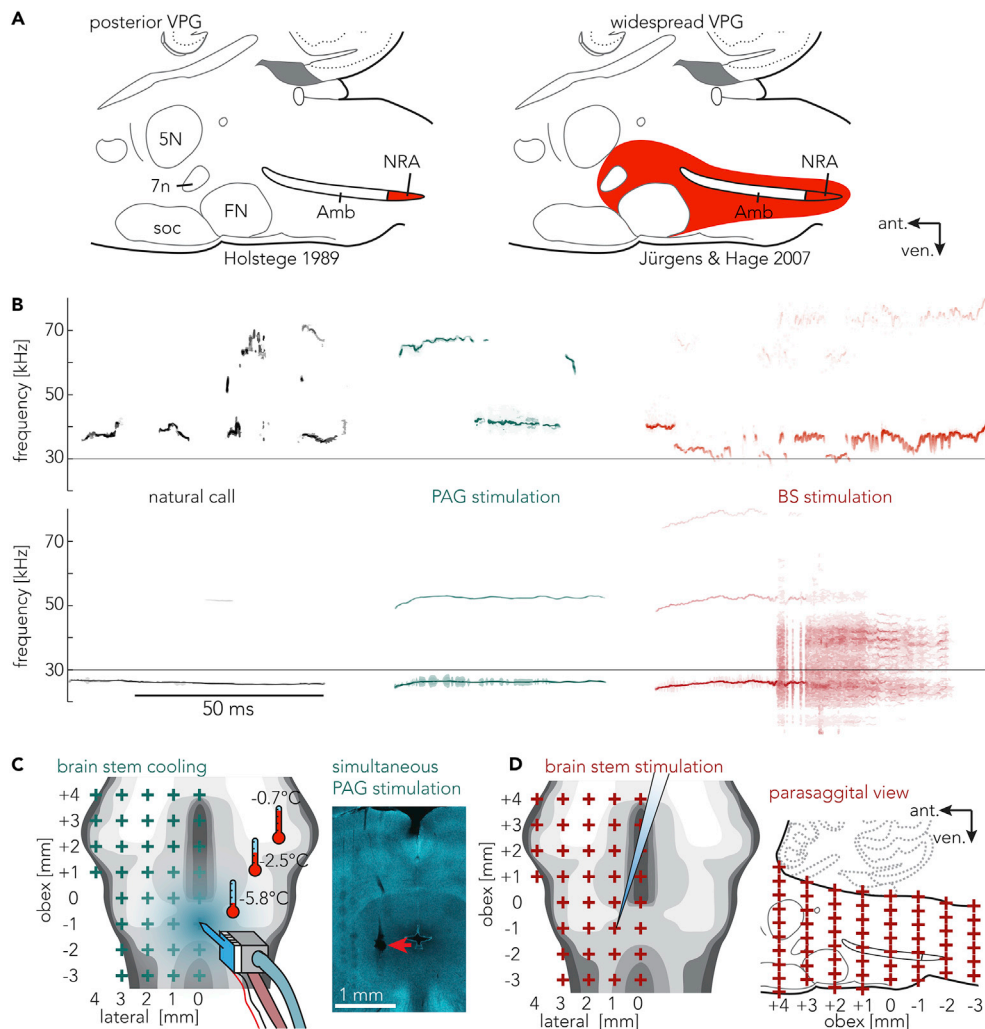
Figure 1. Vocal Pattern Generator Hypotheses, Rat Vocalizations, Stimulation-Evoked Vocalizations, and Local Brainstem Cooling

(A) Competing hypotheses about the mammalian vocal pattern generator superimposed to a schematic mammalian (rat) brainstem. Red areas depict the assumed location of the vocal pattern generator. Left: nucleus retroambiguus as the VPG (adapted from Holstege 1989). Right: dedicated VPG across the ventrolateral pontine brainstem according to Jürgens and Hage (2007). 5N, motortrigeminal nucleus; 7n, facial nerve; Amb, nucleus ambiguus; FN, facial nucleus; NRA, nucleus retroambiguus; soc, superior olivary complex.

(B) Vocalizations of a rat. Top: high-frequency calls, e.g., >30 kHz. Bottom: low-frequency calls, e.g., <30 kHz. Black: species-specific calls of an awake, behaving animal. Teal: vocalizations triggered by electrical microstimulation of the PAG in an anesthetized rat. Red: vocalizations triggered by electrical microstimulation in the brainstem in an anesthetized rat. Note the unnatural shaped vocalizations evoked by direct brainstem stimulation, reflecting the stimulation pattern in the vocalization itself. High- and low-frequency calls evoked by PAG/brainstem stimulation stem from different stimulation sites in the respective areas. High- and low-frequency calls could be evoked at the same PAG location, as shown in example calls of Figure 4.

(C) Left: PAG stimulation and simultaneous, local cooling of the brainstem. Thermistors measuring the temperature on the contralateral side of the brainstem. Blue haze indicates cooling effect. Red crosses indicate the 36 positions arranged in a 1 × 1-mm grid above the brainstem. Scaling and orientation are identical with maps in Figures 2 and 4. Right: coronal section of the PAG with the red arrow indicating the site of stimulation and lesion.

(D) Left: direct stimulation of the brainstem using a tungsten electrode in the same locations as the cooling. Right: depth stimulation of the brainstem was done in 500-μm steps throughout the brainstem.

data, causation and necessity studies spanning across the brain stem could contribute valuable information to the organization of the VPG. We therefore made a new attempt for mapping the mammalian VPG in rats.

Recent focus on rodent vocalizations (Neff, 2019; Okobi et al., 2019; Tschida et al., 2019) underlines the need of a better understanding of the rodent VPG. Rats are highly vocal animals and emit two broad categories of ultrasonic vocalizations (USVs) (Burgdorf et al., 2008): higher-frequency (>30 kHz) calls often associated with positive emotional content and lower-frequency (<30 kHz) calls often associated with fear and alarm (Figure 1B) (Brudzynski, 2005; Knutson et al., 2002).

We took the following measures for a maximally controlled mapping of this structure: (1) We studied calls evoked by midbrain (periaqueductal gray, PAG) stimulation in anesthetized animals, which allowed us to study many hours of uninterrupted stimulation-evoked calling in numerous preparations (Figure 1B). (2) We removed the cerebellum and visualized the brainstem under a surgical microscope, which provided reproducible sub-millimeter precision access to the brainstem. (3) We employed localized cooling as pioneered by Long and Fee (2008). Local cooling powerfully affects vocalization generation and allows for a high-resolution mapping (Figure 1C). (4) We applied a systematic microstimulation mapping of brain stem circuits (Figure 1D).

We find an excellent agreement of localized cooling and stimulation effects. Although the data support the idea that both posterior structures (NRA) and anterior structures (parvicellular reticular formation) contribute to pattern generation in rat vocalizations, the data refute distributed VPG model. Lastly, we reveal major functional differences between the anterior and posterior part of the VPG.

RESULTS

Electrical Stimulation in the Periaqueductal Gray and Brain Stem Evokes Vocalizations

We investigated the localization of the vocal pattern generator (VPG) in the mammalian brain. To do so, we evoked species-specific calls under urethane anesthesia by periaqueductal gray (PAG) stimulation (Figure 1B) and simultaneously applied local cooling (Figure 1C). Single PAG stimulations evoked bouts of 3.5 ± 1.3 (mean $\pm$ SD) calls. As far as we could tell, removal of the cerebellum had no major effect on call production (Figure S1). Calls could be in the high- (>30 kHz) or low-frequency range (<30 kHz, Figure 1B); in a subset of experiments PAG stimulation evoked a series of both high- and low-frequency calls. Call type and number stayed constant for minutes to hours, and only trials with constant calling patterns were used for further analysis. We included an average of 20 ± 7 (mean $\pm$ SD) sites of 5 experiments resulting in 98 total sites. The spatial distribution of these cooling sites is shown in Figure 1C.

In a second set of experiments, we applied electrical microstimulation (Figure 1D) directly to the brainstem, in the same 1 × 1-mm grid as the cooling. We stimulated in total 246 locations on the frontal plane in 8 male rats, on average 30.8 ± 1.7 sites per rat and evoked calls in 98 sites, averaging 12.3 ± 1.3 (mean $\pm$ SEM) sites per rat. Stimulation was performed at the same locations as the cooling (Figure 1D) and additionally at different depths (500 µm steps) at each location. Including the depth z axis, we evoked calls in 195 locations, on average 24.4 ± 3.3 per animal (mean $\pm$ SEM). Contrary to the bouts of calls evoked by PAG stimulation, brain stem stimulation only evoked single vocalizations with durations different from PAG stimulations (Figure S1).

Cooling Effects on PAG-Evoked Calls

Cooling of the brainstem had a multitude of effects on PAG stimulation-triggered vocalizations. In the cooled condition, the number, amplitude, and duration of calls were reduced (Figure 2A). Often, calls got fragmented and interrupted, and in a subset of cases, they were completely abolished. In most instances calls recovered after the offset of cooling along with a rewarming of the brain stem. Maps corresponding to Figure 2A for maximum amplitude and call duration can be found in Figure S2. Across all cooling experiments and all locations, we found that PAG stimulation evoked fewer calls during cooling (1.1 ± 1.1 calls less, mean $\pm$ SD).

Two Discrete Brain Stem Regions Affect Rat Vocalizations

We noticed an inhomogeneous distribution of call reduction upon cooling (Figure 2A). When stimulating the brainstem directly, a similar, bipartite distribution of call evoking sites can be observed (Figure 2B). Average
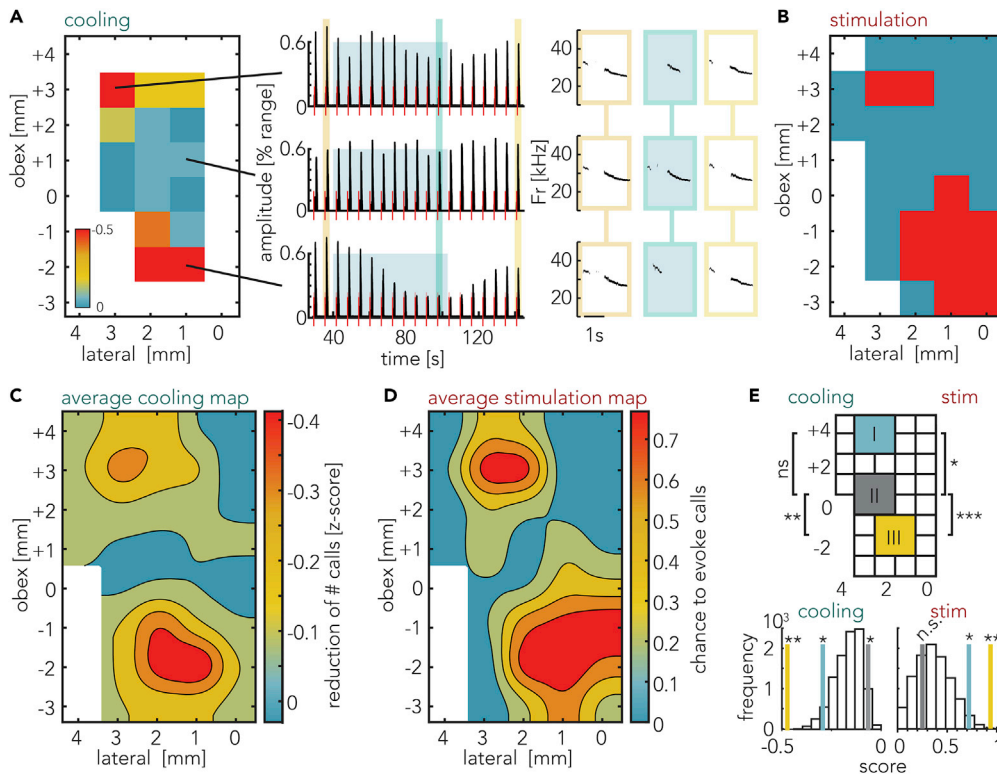
Figure 2. Two Discrete Locations in the Brainstem Affect Vocalizations

(A) Cooling effects on evoked calls. Left: map of the left brainstem surface presenting cooling effects on call numbers. The measures are taken relative to obex (obex: −13.5 mm [posterior] to Bregma and 0 mm lateral). In the sagittal axis, positive coordinates indicate location anterior to obex and negative coordinates indicate location posterior to obex. The heatmap shows the Z score of the effect of cooling on the call numbers following a stimulation, negative values (red) represent a reduction of call numbers. The white areas have not been sampled in this animal. Middle: amplitude of three cooling locations (indicated by the lines) in the same experiment, y axis depicts relative signal strength as a fraction of the detection range of the microphone settings. The observed reduction of amplitude corresponds to a drop of 3.8 dB for the top trace, 0.2 dB for the center trace, and 11.3 dB for the bottom trace, each calculated between the last three trials before cooling and the last three trials during cooling. The red bars indicate onsets and durations of electrical PAG stimulations. The blue backdrop indicates onset and duration of cooling. The yellow and blue bars indicate calls depicted on the right plot. Right: spectrograms of calls before cooling, late cooling, and rewarming as indicated by the respective colors in the waveform plot to the left. Note the strong reduction of call amplitude and duration during cooling of the anterior (top trace) and posterior (bottom trace) locations, but not during cooling of the intermediate location (middle trace).

(B) Map of brainstem stimulation effects from an example animal. Two distinct areas evoked calls upon stimulation. Orientation and scale as in (A). Red indicates locations where calls could be triggered, blue where no calls were triggered. White areas have not been stimulated in this animal.

(C) Average map of the effect of localized brainstem cooling. Depicted is the reduction of evoked calls during the last three stimulation trials compared against the last three trials prior to cooling onset. For each experiment the Z score was calculated and then averaged across experiments. Orientation and scale as in (A).

(D) Mean response to direct brainstem stimulation. Orientation and scale as in (A). Depth data not taken into account. Unsmoothed version of Figures 2C and 2D are depicted in Figure S2.

(E) Top: comparison of different regions on the brainstem with (I) located anterior, (II) medial, and (III) posterior. The grid aligns with the map of (C) and (D). There is a significant difference in the effect of cooling between the three regions (Friedmann, p = 0.0156). The results of the Tukey-Kramer test are detailed in the text. During stimulation, regions differed in the likelihood to evoke calls (Friedmann, p = 0.0006). Bottom: random shuffling of data and comparison against the measured values for each region. Bottom left: the anterior (yellow) and posterior regions (blue) showed a stronger reduction of calls (random shuffling, p = 0.0475 and p = 0.001, respectively). The central (gray) region showed less call number reduction than the randomly shuffled data (random shuffling, p = 0.0406). Bottom right: for stimulation, both the anterior region as well as the posterior region showed a significantly higher rate of evoked calls (random shuffling, p = 0.03 and p = 0.00005, respectively). The center region did not differ from the shuffled data.
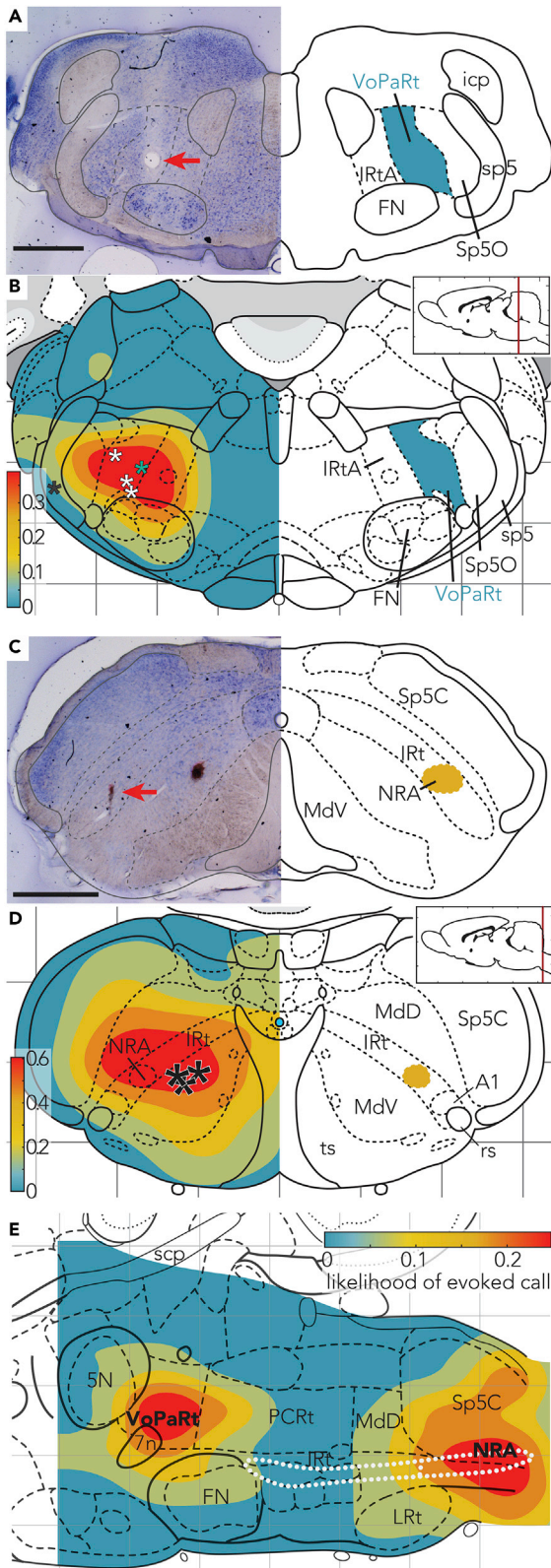
Figure 3. The Anterior Region of the VPG Corresponds to the Parvicellular Reticular Formation that We Term the VoPaRt, whereas the Posterior Region Maps to the NRA and Its Close Surrounding

(A) Coronal section with Nissl staining. Lesion (red arrow) in the anterior part, −10.80 mm from bregma. Scale bar, 1 mm. On the right, identified regions are drawn.

(B) Coronal map of the average vocalization rate as response of brainstem stimulation. Asterisks indicate lesions placed at sites of strongest responses across animals (single black asterisk indicates a lesion placed 1 mm lateral of the strongest response). In the anterior-posterior axis, lesions ranged from bregma −10.50 mm to bregma −11.16 mm. Lesions have been overlayed with the coronal section of bregma −10.80 from Paxinos & Watson Rat Brain Atlas for illustration purposes.

(C) Coronal section with Nissl staining. Lesion (red arrow) in the posterior part −14.52 mm from bregma. Scale bar, 1 mm.

(D) Average depth response rate to brainstem stimulation superimposed with the Paxinos brain atlas −15.00 mm posterior of bregma. Lesions ranged from −14.52 to −15.72 mm posterior of bregma.

(E) Parasagittal view of the brainstem with a heatmap showing sites of calls evoked by electrical stimulation. The white, dotted structure shows the nucleus ambiguous and the nucleus retroambiguus (subsection in posterior brainstem).

5N, motor trigeminal nucleus; 7n, facial nerve; A1, A1 noadrenaline cells; FN, facial nucleus; icp, inferior cerebellar pedunculus; IRtA, intermediate reticular nucleus alpha part; IRt, intermediate reticular nucleus; LRt, Lateral reticular nucleus; MdD, medullary reticular nucleus dorsal part; MdV, medullary reticular nucleus ventral part; rs, rubospinal tract; Sp5C, Spinal trigeminal tract caudal part; Sp5O,Spinal trigeminal tract oral part; sp5, spinal trigeminal tract; soc, superior olivary complex; ts, tectospinal tract.

maps of all experiments of both the cooling (Figure 2C) as well as stimulation (Figure 2D) experiments reaffirm this bipartite distribution. The anterior region affecting calls centered on +3.5 mm anterior and 2.5 mm lateral from obex. The posterior region affecting calls was located 1.5 mm posterior and 1.5 mm lateral from the obex.

In order to assess the spatial heterogeneity of the responses to cooling, we analyzed and compared cooling and stimulation effects between three 2 × 2-mm regions defined along the antero-posterior axis. The anterior and posterior regions were centered on the coordinates mentioned above, and a third region was chosen just in between (Figure 2E top).

There were on average fewer calls per stimulation during cooling the anterior region (1.75 $\pm$ 0.23 calls less) and the posterior region (2.37 $\pm$ 0.27 calls less). Cooling the center region only led to a marginal reduction of 0.3 $\pm$ 0.07 calls. The reduction of calls differed between the regions (Friedmann, p = 0.0183) and was more pronounced for cooling the posterior region than for cooling the central region (Tukey-Kramer, p = 0.0130, Figure 2E top). There was no significant difference between the anterior and the posterior region (Tukey-Kramer, p = 0.33) or between the anterior and the central region (Tukey-Kramer, p = 0.33). To test if the three regions differ from the average response to cooling and if the observed spatial distribution is different from a random distribution, we compared the measured values in our regions against shuffled data. The observed distribution for all regions was significantly different from a random distribution (see Figure 2E bottom left and Methods for details).

In agreement with the distribution of cooling effects, we found that direct stimulation of the anterior region evoked calls in 72% of trials and in the posterior region in 94% of trials (23 and 30 trials of 32 trials, respectively). In contrast, the central region only evoked calls in 17% (5 of 30 trials). The difference between these three regions was significant (Friedmann, p = 0.0006). Anterior and posterior regions evoked more calls than the central region (Tukey-Kramer, p = 0.0206 and p = 0.0005, respectively, Figure 2E top); the difference between anterior and posterior was not significant (Tukey-Kramer, p = 0.53). Compared against randomly distributed data, the anterior and posterior data were significantly different (see Figure 2E bottom right).

The spatial distribution of call reduction induced by cooling and that of the evoked vocalizations by direct electrical stimulations were correlated (Pearson correlation, R = 0.605, p = 0.00012). The excellent spatial correspondence of those maps suggests a highly reproducible fine grain spatial organization of call production in the rat brain stem.

The Two Brain Stem Vocalization Regions Map to Part of the Parvicellular Reticular Formation and the Nucleus Retroambiguus

To assess the anatomical identity of the anterior and the posterior vocalization region we combined stimulation experiments and electrolytic lesions. To this end, we obtained depth data by stimulating from the dorsal surface down to the ventral side of the brainstem in steps of 500 μm. At the site where we could trigger calls with the lowest threshold, we placed a lesion at the end of the experiment. In Figure 3A, a brain section at bregma +10.8 mm is depicted with a red arrow marking the lesion. In total we recovered five lesions, of which four were placed within the posterior subsection of the parvicellular reticular formation alpha part (posterior PCRtA). Figure 3B also shows the response rate to stimulations at different depths at obex +3 superimposed on the Paxinos Brain Atlas. The peak response was around the posterior half of the parvicellular reticular formation alpha part (bregma −10.5 to −11.1 mm; lateral 1.5 to 3.3 mm). We therefore suggest the term VoPaRt (vocalization region of the parvicellular reticular formation) for this anterior part of the VPG.

We also placed lesions at the posterior region (Figure 3C). We recovered three lesions, all close to the NRA. Lesions ranged from −14.52 to −15.72 mm posterior of bregma. Superimposing the likelihood of calls at the obex −2 position, we found the center of the heatmap overlapping with the NRA, further confirming the role of this region in the call production (Figure 3D). We visualized the brain stem stimulation response also in a parasagittal section with the Paxinos brain atlas (Figure 3E).

To further characterize the target structures, we quantified the cross-sectional area of somata from ten chosen regions of the brainstem and found that they were different (Figures 4A–4C, Kruskal-Wallis, p = 5.767×10^{-151}). Specifically, neurons in both VoPaRt and NRA are significantly smaller than neurons in any
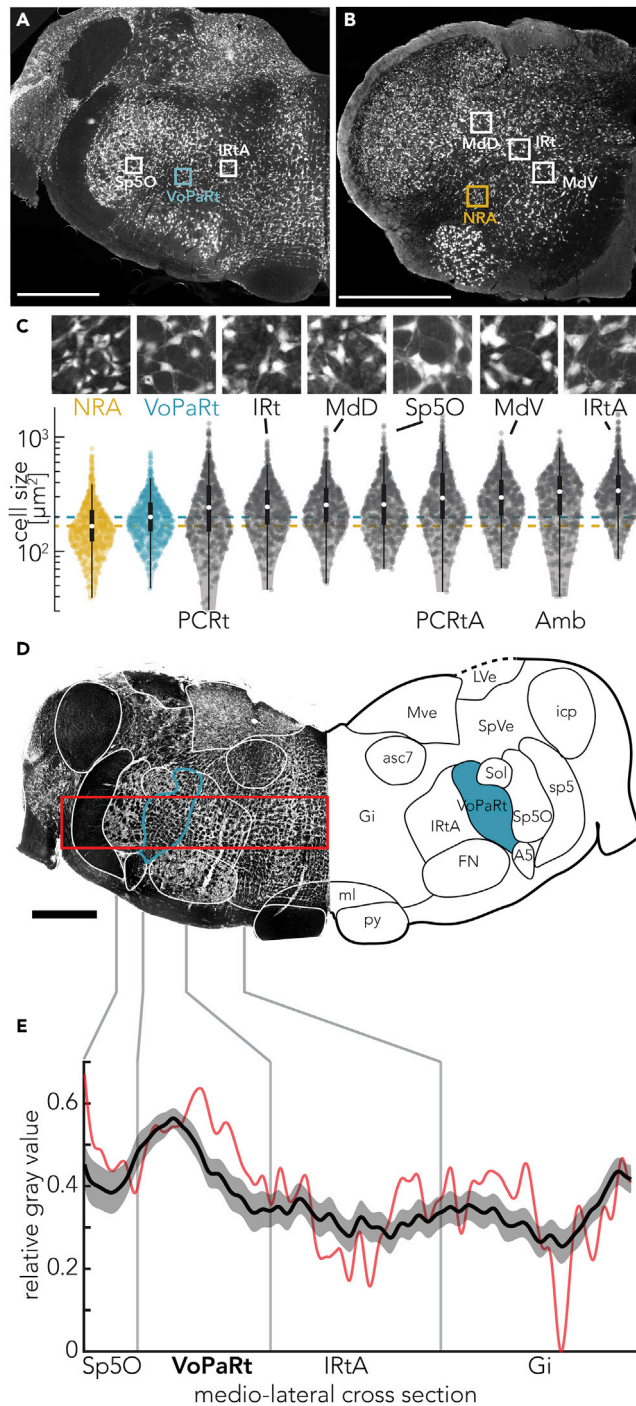
Figure 4. VoPaRt and NRA Consist of Exceptionally Small Cells and the VoPaRt Is Highly Myelinated

(A) NeuN staining of a coronal section of the brainstem around the target area of the anterior VPG region, bregma −11.2 mm. The boxes indicate the locations of magnifications in (C). Scale bar, 1 mm.

(B) NeuN staining of a coronal section of the brainstem around the target area of the posterior VPG region, bregma −14.6 mm. The boxes indicate the locations of magnifications in (C). Scale bar, 1 mm.

(C) Comparison of the cell cross-sectional area ($n_{neurons}$ = 600 per region, $n_{animals}$ = 2). Magnified sections correspond to numbered rectangles in the overview of (F) and (G). Magnified sections are 150× 150 μm. Soma in VoPaRt and NRA are significantly smaller than any other brainstem region measured here; statistical details are summarized in Figure S3 and Table S1. Boxplots overlaid with violin plots depict the soma size for each region. PCRtA lies anterior of the coronal

Figure 4. *Continued*

section in (E) and PCRt and Amb are between the sections of (E) and (F); therefore, all three regions are not shown in (E) or (F).

(D) Myelin-stained coronal section at the height of the VoPaRt, where calls were affected by cooling/evoked by stimulation. The VoPaRt (blue) shows a stronger staining (darker) response than surrounding areas. The red rectangle marks the area used for analysis in (E). Additional abbreviations: A5, A5 noradrenaline cells; asc7,ascending fibers of the facial nerve; Gi, gigantocellular reticular nucleus; LVe, lateral vestibular nucleus; ml, medial lemniscus; Mve, medial vestibular nucleus; py, pyramidal tract; SpVe, spinal vestibular nucleus; Sol, nucleus of the solitary tract.

(E) Quantification of myelinization for VoPaRt and surrounding areas. The black line shows the average myelinization from Sp5O to the midline of the brainstem, normalized to the maximum myelinization of each brain section ($n_{sections}$ = 18, $n_{hemispheres}$ = 6, n_{brains} = 3) analyzed. Gray shading depicts the SEM. The red line is the measurement of the example section presented in (D).

other regions that we sampled (post hoc Tukey-Kramer, Figure S3A and Table S1). Interestingly, neurons in the anterior PCRtA, not part of the VoPaRt, cell body sizes were significantly larger. Also, neurons in the rest of the parvicellular nucleus were larger. In a similar fashion, the NRA neurons were smaller than any other areas we sampled and even smaller than neurons in the directly anterior neighboring nucleus ambiguus. NRA neurons were smaller than neurons in the VoPaRt (Tukey-Kramer test, p = $2.7*10^{-4}$). Furthermore, we found the VoPaRt to be highly myelinated (Figure 4D). Comparing the myelinization against surrounding areas (Figure 4E), we find the myelinization to be significantly higher than that of both the intermediate reticular formation alpha part and the gigantocellular reticular nucleus (Tukey-Kramer, p = 0.0004 and p = 0.0017, respectively). The difference to the Sp5O was not significant (Tukey-Kramer, p = 0.12).

The Anterior VoPaRt Affects High-Frequency Calls and Frequency Modulation, whereas the NRA Affects Flat, Low-Frequency Calls

Having identified two subparts of the VPG, we asked if the VoPaRt and NRA were functionally different. We found that VoPaRt cooling led to a loss of high-frequency calls, i.e., calls with a fundamental frequency higher than 30 kHz (Figure 5A) in 53% of the trials (10 of 19 trials). Cooling in the central region only affected these high-frequency calls in 10% (2 of 21 trials) and cooling the NRA never affected the high-frequency calls selectively (0 of 16 trials). The differences on high-frequency calls between the VoPaRt, center, and NRA region were significant (Friedmann, p = 0.0152), and cooling the VoPaRt showed a significantly stronger reduction in high-frequency calls than the NRA region (Tukey-Kramer, p = 0.013). Cooling reduced the number of high-frequency calls in the VoPaRt more often than it would be expected from a random distribution of the effect (Random shuffling, p = 0.0002, Figure S4A).

In line with these results, we found that stimulating the VoPaRt led to high-frequency calls in 72% of trials (23 of 32 trials, Figure 5B). In contrast, only 16% (5 of 32) of NRA stimulation trials evoked high-frequency calls and 13% in the center region (4 of 30 trials), resulting in a significant difference between the three regions Friedmann, p = 0.00098). VoPaRt stimulation led to more high-frequency calls than stimulation in the NRA or center region (Tukey-Kramer, p = 0.0011 and p = 0.0161, respectively). The distribution of high-frequency call-evoking sites was further different from a random distribution (Random shuffling, p = 0.0002, see Figure S4B). The spatial distribution of cooling and stimulation effects correlate significantly (Pearson's correlation, R = 0.553, p = 0.00057). We conclude that the VoPaRt is involved specifically in the production of high-frequency vocalizations.

In contrast to the effect on high-frequency calls, we found that the NRA cooling predominantly affected low-frequency calls (Figure 5C). NRA cooling reduced low-frequency calls in 94% trials (15 of 16 trials), whereas VoPaRt cooling only reduced low frequencies in 26% of trials (5 of 19 trials). Cooling the center region affected low-frequency calls in 14% (3 of 21 trials). These differences were significant (Friedmann, p = 0.022) with the NRA cooling inhibiting significantly more than the center region (Tukey-Kramer, p = 0.017, see Figure S4C for random shuffling tests).

Accordingly, NRA stimulation led to low-frequency calls in 91% of cases (29 of 32 trials) but only in 6% and 10% when stimulating in the VoPaRt or central region, respectively (2 of 32 trials for VoPaRt and 3 of 30 trials in center region) (Figure 5D). The difference was significant (Friedmann, p = 0.00079), with NRA stimulation evoking more low-frequency calls than stimulation in either the VoPaRt or the center region
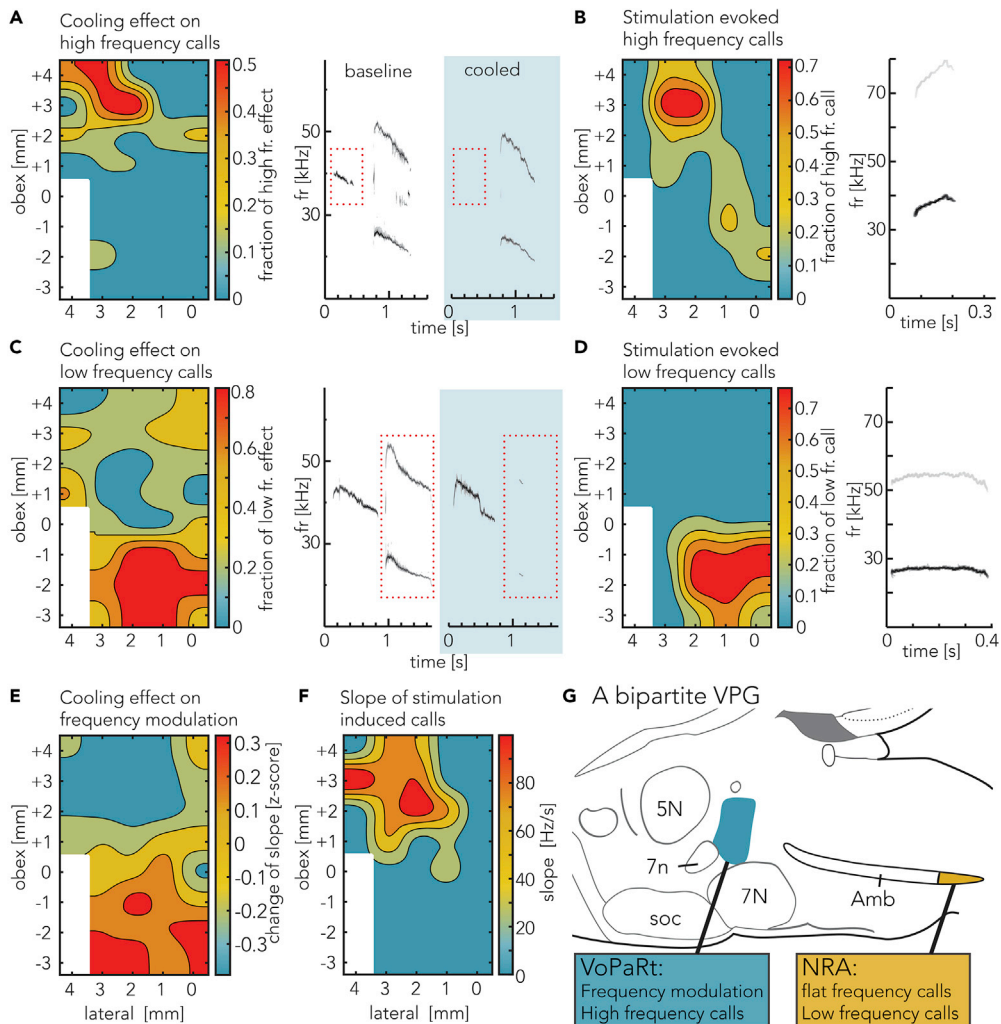
Figure 5. The Identified Anterior Region Selectively Affects High-Frequency and Frequency-Modulated Calls, whereas the Posterior Region Selectively Affects Low-Frequency Calls

(A) Left: average effect on high-frequency calls (>30 kHz) of brainstem cooling. Right: example calls before and during late cooling. High-frequency calls vanish, whereas the low-frequency calls and their harmonics (vertically shifted) are unaffected.

(B) Probability map of locations where stimulation triggered high-frequency calls. High-frequency calls are predominantly evoked in the anterior brainstem (VoPaRt region). Right: example call.

(C) Left: average effect on low-frequency calls (<30 kHz) of brainstem cooling. Right: example calls before and during cooling. More example calls are shown in Figure S5. Low-frequency calls and their respective harmonics are strongly affected, whereas high-frequency calls are unaffected.

(D) Probability map of locations where stimulation triggered low-frequency calls. Low-frequency calls are predominantly evoked in the posterior brainstem (NRA region). Right: example call.

(E) Average change of slopes during cooling trials depicted as the Z score. Red indicates an increase of slope due to cooling, whereas blue indicates a decrease of slope. Example calls can be found in Figure S5.

(F) Average, absolute slope of calls triggered by brainstem stimulation. Red indicates a call with a steep slope, whereas blue indicates a flat call. For example calls, view example calls from (B) and (D) in this figure.

(G) Our suggested model of the bipartite vocal pattern generator in the rat brainstem. Two regions are involved. The VoPaRt is located in the alpha part of the parvicellular reticular formation and has a range of about 700 μm anterior-posterior centered at bregma −10.80 mm posterior of bregma. The second region is the NRA and possibly its direct surroundings at bregma −15.00 mm. Furthermore, the VoPaRt is involved with modulated, high-frequency calls and the NRA with flat and low-frequency calls.

(Tukey-Kramer, p = 0.005 and p = 0.0019, respectively). Random shuffling test confirmed the non-random distribution of these effects and is depicted in Figure S4D). The distribution of cooling and stimulation effects were correlated (Pearson's correlation, R = 0.677, p = 0.000008), supporting the interpretation that the two methods, cooling and stimulation, indeed affect the same circuitry in the brain stem.

To quantify the specific regional effects on high and low frequencies in a combined, robust analysis, we sampled a subset of experiments, where PAG stimulation reliably evoked both high- and low-frequency calls after each stimulation. This analysis was done for the VoPaRt, NRA, and center regions (see Methods). A comparison of Z scores for the cooling effect in the three regions confirmed the results obtained by the manual scoring and are summarized in Figure S6. Summarizing, we found cooling the VoPaRt significantly more strongly reduced high-frequency than low-frequency calls (t test, p = 0.0022). In contrast, cooling of the NRA reduced low-frequency calls significantly more strongly than high-frequency calls (t test, p = 0.005). The center region did not show a difference.

To analyze cooling and stimulation effects on the frequency modulation of calls we analyzed the start and end frequency of five calls before cooling and five calls at the end of cooling and calculated the absolute, average Hz per second change (slope) of each call. Therefore, slope is a simplified measure of the frequency modulation of a call, quantifying the absolute change of frequency per second. The difference between the mean slope before and at the end of cooling is shown as a map in Figure 5E as the Z score. In the VoPaRt area, we find that the slope of calls decreased by 6.09 ± 0.96 Hz.s^{-1} (mean $\pm$ SEM) when cooling is applied (example in Figure S5C). By cooling the NRA, the slope of calls was increased by 5.48 ± 0.74 Hz.s^{-1} and was significantly different from the VoPaRt (Friedman, p = 0.0183, Tukey-Kramer, p = 0.013) (example in Figure S5D). Compared against randomly distributed data, the VoPaRt showed a significant decrease of call slope, whereas cooling the NRA region showed a significant increase in slope (random shuffling, p = 0.0002 and p = 0.0123, respectively, see Figure S4E). Those results indicate that cooling the anterior region (VoPaRt) reduced call frequency modulation, whereas cooling the posterior region (NRA) enhanced call frequency modulation.

This result is confirmed by measuring the average slope of stimulation-evoked calls. Calls evoked by stimulation of the VoPaRt region had slopes of 90.9 ± 8.5 Hz.s^{-1} (mean $\pm$ SEM, Figure 5F) and were distinct from the calls evoked by NRA stimulation, which had average slopes of 9.49 ± 0.95 Hz.s^{-1} (Wilcoxon sign rank, p = 0.0078). Compared with randomly distributed data, calls evoked by stimulating the VoPaRt showed a higher modulation and calls evoked by stimulating the NRA region showed less modulation (random shuffling, p = 0.021 and p = 0.0111, respectively, see Figure S4F). The results from the cooling and stimulation were negatively correlated (Pearson's correlation, R = −0.7564, p = 0.000019), confirming the spatial similarity of the effects on call modulation.

A Functionally and Anatomically Bipartite Vocal Pattern Generator

Summarizing our findings, we propose the model for the vocal pattern generation in the rat brainstem in Figure 5G. Thus, the rodent VPG consists of a bipartite system including the vocalization region of the parvicellular reticular formation (VoPaRt) and the NRA. The VoPaRt is predominantly involved in the production of high-frequency, frequency-modulated calls. The NRA on the other hand is involved in the production of low-frequency flat calls.

DISCUSSION

We studied the rat's brainstem vocal pattern generation either by looking at the influence of local brainstem cooling on calls evoked by electrical stimulations of the periaqueductal gray or directly via brainstem electrical stimulations. We find a fine-grain, highly reproducible organization of vocalization involved areas in the brainstem. Our data suggest the rat vocal pattern generator is bipartite. The anterior part of the vocal pattern generator localizes to the posterior parvicellular reticular formation alpha part and appears to be predominantly involved in frequency-modulated high-frequency calls. The posterior part of the vocal pattern generator localizes to the NRA and appears to be predominantly involved in low-frequency, non-modulated calls.

The Rat Brainstem Contains a Vocal Pattern Generator

Our results agree with a huge body of work from numerous species that points to the existence of vocal pattern generator circuits in the mammalian brain stem. (1) Thus, as others before, we find that the brain stem is necessary for call production and that cooling of various brain stem sites aborts calls. This result

agrees with chemical inactivation (Shiba et al., 1997) and dissection studies (Zhang et al., 1995) that suggested that the brain stem is necessary for mammalian vocalizations. (2) We confirm that the brainstem affects a wide variety of calls (Dressnandt and Jürgens, 1992) and various aspects of call production (Sugiyama et al., 2010). (3) We find that the brainstem is involved in elementary aspects of call production. Accordingly, brainstem stimulation-evoked vocalizations, in sharp contrast to the upstream periaqueductal gray, do not match up with natural calls but consist of elementary non-natural vocalization. (4) Finally, the brainstem structures identified here are not simply laryngeal or respiratory vocalization output neurons, but instead we identified structures upstream of such motoneuron pools (Cunningham and Sawchenko, 2000; Hannig and Jürgens, 2005; Thoms and Jürgens, 1987).

A Bipartite Model of the Vocal Pattern Generator

A variety of models of the vocal pattern generator have been suggested (Figure 1A), and our data support certain aspects as well as reject others. We suggest a new model organization of the vocal pattern generator circuits (Figure 5G). In agreement with Holstege (1989) we find a critical contribution of NRA (Figure 1A, left) to vocal pattern generation in the rat. At the same time our data suggest that the NRA is not the sole VPG in rats. In agreement with data from squirrel monkeys (Hage and Jürgens, 2006b) we also observed a critical contribution of an anterior region (Figure 1A right) to vocal pattern generation in the rat; we identify this region as a subsection of the parvicellular region of the reticular formation (VoPaRt). Our data do not support the idea of a spatially extended VPG as proposed before (Jürgens and Hage, 2007; Sugiyama et al., 2010) (Figure 1A right, red), however. Both our stimulation and our cooling data are incompatible with the critical prediction of this model, namely, a continuous distribution of vocalization effects along the anterior-posterior axis. A major insight from our work is that the anterior VoPaRt region and the posterior NRA parts of the VPG do not seem to be functionally equivalent.

The Anterior Vocal Pattern Generator Region in the Parvicellular Reticular Formation Contributes to Frequency-Modulated High-Frequency Calls

Our data agree with several studies indicating an anterior location of the VPG, somewhere in the reticular formation (Dressnandt and Jürgens, 1992; Hage and Jürgens, 2006b; Jürgens, 2000; Siebert and Jürgens, 2003; Zhang et al., 1995). Our results extend the conclusion of these studies in two major ways. First, we clarify the exact histological identity of the region as the posterior part of the alpha-nucleus of the parvicellular reticular formation. Such histological identification also allowed us to show that this vocalization region is made up of very small cells. The small cell size of VoPaRt neuron is somewhat surprising at first sight given that this region probably has diverse and far-reaching connections; we wonder if small cell size and the associated short membrane time constants might contribute to high-speed processing for rat vocalization patterns, which are modulated on the millisecond timescale, with muscle contractions as high as 150 Hz in the vocal tract (Riede, 2011). It has been shown that small cells with their comparable small membrane surfaces have a small membrane capacity and thus short time constants. Thus, cerebellar granular cells, which are among the smallest neurons in the mammalian brain, have very short time constants (Brickley et al., 2001; D'Angelo et al., 1995; Silver et al., 1992). The cellular time constant is a major but not the only factor determining processing speed; for review see Koch et al. (1996). We find it therefore likely that the small size of VoPaRt and NRA neurons has functional implications for processing speed. The small cell sizes are further emphasized by the difference in cell size between the anterior section of the PCRtA and the VoPaRt. Another important feature of processing speed is myelinization, and we found the VoPaRt to be highly myelinated, more so than the intermediate reticular nucleus, directly besides it, further strengthening the hypothesis of high-speed processing in the VPG. The second insight from our work is that VoPaRt does not seem to contribute to all vocalizations equally but according to both cooling and stimulation data seems to be particularly relevant for high-frequency calls and frequency modulation. Differential effects on call types have been indicated in lesion studies in squirrel monkeys. PAG stimulation triggered vocalizations in anesthetized monkeys, comparable with our study. By injection of kynurenic acid in the periolivary region (presumably the region homologous to VoPaRt), calls with a strong frequency modulation were stopped, but other calls were unaffected (Jürgens, 2000). In bats echolocation calls have been inhibited by injection of kynurenic acid into the paralemniscal area, whereas the lower-frequency communication calls were unaffected (Fenzl and Schuller, 2005). Intriguingly, there is also evidence from recording studies in monkeys (Hage and Jürgens, 2006a) that call-related activity in the anterior VPG region is specific to high-frequency, frequency-modulated calls.

The Posterior Vocal Pattern Generator Corresponds to the Nucleus Retroambiguus and Contributes to the Low-Frequency, Flat-Frequency Calls

As already discussed above, our result that the NRA plays a critical role in vocal pattern generation is in full agreement with earlier studies. Our analysis added aspects, however. First, we find that NRA cells, much like neurons in the VoPaRt, are exceptionally small. The concurrence of these two results makes us wonder if small cell size is a signature of VPG structures. Second, we find that the NRA does not contribute to all vocalizations equally. Both cooling effects and stimulation indicate that the NRA is particularly relevant for low-frequency, non-frequency-modulated sounds. Thus, we support that the VPG has a functionally dedicated structure, as suggested by Hage and Jürgens (2006a).

Mechanisms of Call Generation

What do these results tell us about how calls are generated? In a series of elegant experiments Long and Fee (2008) introduced the cooling tools to study the role of avian HVC in song control. In this seminal publication, the authors describe a dilation of the zebra finch song upon cooling of the song production pathway (HVC and RA). Thus, these experiments suggested that the HVC might work like a clock in the millisecond range for song control. In our experiments we did not find a dilation of the vocalizations. Instead, we consistently observed a reduction of call duration and sometimes breaking of calls. Comparable syllable breaking was also observed upon stronger cooling of the birdsong motor pathway (Goldin et al., 2013). In our experiments, cooling of the VPG structures resulted in a breaking of the neural circuits underlying the call production and resulting in an interrupted call production. Thus, we do not think that VoPaRt or NRA functions as "clocks" for call production. If anything, these structures seem to function as "drivers" for call production, a cooling of which results in call shortening, breaking, and call loss.

Another insight from our work seems to be that the circuits forming the bipartite mammalian VPG seem to be highly conserved. The predictive power of vocal pattern generation data from monkeys and cats for the functional organization in the rat is certainly astounding.

A Bipartite Vocal Pattern Generator and the Functional Dichotomy of Rat Ultrasonic Vocalizations

What are the functional implications of our results? The first thing that comes to mind is that the functional division of the rat VPG into an anterior high-frequency/frequency-modulation VoPaRt region and a posterior low-frequency NRA division matches up with a functional dichotomy in rat vocalizations. As a coarse first-order approximation rat vocalizations can be divided into high-frequency, often frequency-modulated, calls (often referred to as 50-kHz ultrasonic vocalizations), which communicate positive affect and into low-frequency, often flat calls (referred to as 22-kHz ultrasonic vocalizations), which communicate negative affect/fear/alarm (Brudzynski, 2005; Knutson et al., 2002; Panksepp and Burgdorf, 2003; Schwarting et al., 2007). Dividing the VPG into two subregions that generate sound of opposite valence could greatly simplify the wiring of the rat nervous system and avoid the need of multiplexing opposing messages through the same vocalization centers.

Limitations of the Study

Neuronal recordings could strengthen the results presented here but go beyond the scope of this publication. Experiments with awake animals could strengthen the results further but are methodologically difficult.

Resource Availability

Lead Contact

Requests for further information should be directed to and will be fulfilled by the Lead Contact, Michael Brecht (michael.brecht@bccn-berlin.de).

Materials Availability

This study did not generate new unique reagents.

Data and Code Availability

The dataset and code generated during this study will be available upon request from the corresponding author.

METHODS

All methods can be found in the accompanying Transparent Methods supplemental file.

SUPPLEMENTAL INFORMATION

Supplemental Information can be found online at https://doi.org/10.1016/j.isci.2020.101804.

AUTHORS CONTRIBUTION

Conceptualization, Methodology, Investigation, Formal Analysis, Writing, K.H. and M.B.; Visualization, K.H.; Supervision, M.B.

DECLARATION OF INTERESTS

The authors declare no competing interests.

REFERENCES

Bennett, P.J.G., Maier, E., and Brecht, M. (2019). Involvement of rat posterior prelimbic and cingulate area 2 in vocalization control. Eur. J. Neurosci. 50, 3164–3180.

Brickley, S.G., Revilla, V., Cull-Candy, S.G., Wisden, W., and Farrant, M. (2001). Adaptive regulation of neuronal excitability by a voltage-independent potassium conductance. Nature 409, 88–92.

Broca, P. (1861). Remarks on the seat of the faculty of articulated language, following an observation of aphemia (loss of speech). Bull. Soc. Anat. 6, 330–357.

Brudzynski, S.M. (2005). Principles of rat communication: quantitative parameters of ultrasonic calls in rats. Behav. Genet. 35, 85–92.

Burgdorf, J., Kroes, R.A., Moskal, J.R., Pfaus, J.G., Brudzynski, S.M., and Panksepp, J. (2008). Ultrasonic vocalizations of rats (Rattus norvegicus) during mating, play, and aggression: behavioral concomitants, relationship to reward, and self-administration of playback. J. Comp. Psychol. 122, 357–367.

Cunningham, E.T., and Sawchenko, P.E. (2000). Dorsal medullary pathways subserving oromotor reflexes in the rat: implications for the central neural control of swallowing. J. Comp. Neurol. 417, 448–466.

D'Angelo, E., De Filippi, G., Rossi, P., and Taglietti, V. (1995). Synaptic excitation of individual rat cerebellar granule cells in situ: evidence for the role of NMDA receptors. J. Physiol. 484, 397–413.

Dressnandt, J., and Jürgens, U. (1992). Brain stimulation-induced changes of phonation in the squirrel monkey. Exp. Brain Res. 89, 549–559.

Fay, R.A., and Norgren, R. (1997). Identification of rat brainstem multisynaptic connections to the oral motor nuclei using pseudorabies virus: III. Lingual muscle motor systems. Brain Res. Rev. 25, 291–311.

Fenzl, T., and Schuller, G. (2005). Echolocation calls and communication calls are controlled differentially in the brainstem of the bat Phyllostomus discolor. BMC Biol. 3, 17.

Goldin, M.A., Alonso, L.M., Alliende, J.A., Goller, F., and Mindlin, G.B. (2013). Temperature induced syllable breaking unveils nonlinearly interacting timescales in birdsong motor pathway. PLoS One 8, e67814.

Hage, S.R., and Jürgens, U. (2006a). On the role of the pontine brainstem in vocal pattern generation: a telemetric single-unit recording study in the squirrel monkey. J. Neurosci. 26, 7105–7115.

Hage, S.R., and Jürgens, U. (2006b). Localization of a vocal pattern generator in the pontine brainstem of the squirrel monkey. Eur. J. Neurosci. 23, 840–844.

Hannig, S., and Jürgens, U. (2005). Projections of the ventrolateral pontine vocalization area in the squirrel monkey. Exp. Brain Res. 169, 92.

Holstege, G. (1989). Anatomical study of the final common pathway for vocalization in the cat. J. Comp. Neurol. 284, 242–252.

Jürgens, U. (1994). The role of the periaqueductal grey in vocal behaviour. Behav. Brain Res. 62, 107–117.

Jürgens, U. (2000). Localization of a pontine vocalization-controlling area. J. Acoust. Soc. Am. 108, 1393–1396.

Jürgens, U., and Hage, S.R. (2007). On the role of the reticular formation in vocal pattern generation. Behav. Brain Res. 182, 308–314.

Jürgens, U., and Ploog, D. (1970). Cerebral representation of vocalization in the squirrel monkey. Exp. Brain Res. 10, 532–554.

Jürgens, U., and Richter, K. (1986). Glutamate-induced vocalization in the squirrel monkey. Brain Res. 373, 349–358.

Knutson, B., Burgdorf, J., and Panksepp, J. (2002). Ultrasonic vocalizations as indices of affective states in rats. Psychol. Bull. 128, 961–977.

Koch, C., Rapp, M., and Segev, I. (1996). A brief history of time (constants). Cereb. Cortex 6, 93–101.

Kyuhou, S., and Gemba, H. (1998). Two vocalization-related subregions in the midbrain periaqueductal gray of the Guinea pig. Neuroreport 9, 1607–1610.

Long, M.A., and Fee, M.S. (2008). Using temperature to analyse temporal dynamics in the songbird motor pathway. Nature 456, 189–194.

Lu, C.-L., and Jürgens, U. (1993). Effects of chemical stimulation in the periaqueductal gray on vocalization in the squirrel monkey. Brain Res. Bull. 32, 143–151.

Lüthe, L., Häusler, U., and Jürgens, U. (2000). Neuronal activity in the medulla oblongata during vocalization. A single-unit recording study in the squirrel monkey. Behav. Brain Res. *116*, 197–210.

Neff, E.P. (2019). Neural control of duets between Alston's singing mice, an emerging vocalization model. Lab Anim. *48*, 137.

Okobi, D.E., Banerjee, A., Matheson, A.M.M., Phelps, S.M., and Long, M.A. (2019). Motor cortical control of vocal interaction in neotropical singing mice. Science *363*, 983–988.

Panksepp, J., and Burgdorf, J. (2003). "Laughing" rats and the evolutionary antecedents of human joy? Physiol. Behav. *79*, 533–547.

Riede, T. (2011). Subglottal pressure, tracheal airflow, and intrinsic laryngeal muscle activity during rat ultrasound vocalization. J. Neurophysiol. *106*, 2580–2592.

Sakata, J.T., Woolley, S.C., Fay, R.R., and Popper, A.N. (2020). The Neuroethology of Birdsong (Springer).

Schwarting, R.K.W., Jegan, N., and Wöhr, M. (2007). Situational factors, conditions and individual variables which can determine ultrasonic vocalizations in male adult Wistar rats. Behav. Brain Res. *182*, 208–222.

Shiba, K., Umezaki, T., Zheng, Y., and Miller, A.D. (1997). The nucleus retroambigualis controls laryngeal muscle activity during vocalization in the cat. Exp. Brain Res. *115*, 513–519.

Siebert, S., and Jürgens, U. (2003). Vocalization after periaqueductal grey inactivation with the GABA agonist muscimol in the squirrel monkey. Neurosci. Lett. *340*, 111–114.

Silver, R.A., Traynelis, S.F., and Cull-Candy, S.G. (1992). Rapid-time-course miniature and evoked excitatory currents at cerebellar synapses in situ. Nature *355*, 163–166.

Sugiyama, Y., Shiba, K., Nakazawa, K., Suzuki, T., and Hisa, Y. (2010). Brainstem vocalization area in Guinea pigs. Neurosci. Res. *66*, 359–365.

Thoms, G., and Jürgens, U. (1987). Common input of the cranial motor nuclei involved in phonation in squirrel monkey. Exp. Neurol. *95*, 85–99.

Tschida, K., Michael, V., Takatoh, J., Han, B.-X., Zhao, S., Sakurai, K., Mooney, R., and Wang, F. (2019). A specialized neural circuit gates social vocalizations in the mouse. Neuron *103*, 459–472.e4.

Zhang, S.P., Bandler, R., and Davis, P.J. (1995). Brain stem integration of vocalization: role of the nucleus retroambigualis. J. Neurophysiol. *74*, 2500–2512.

Supplemental Information

A Functionally and Anatomically Bipartite

Vocal Pattern Generator

in the Rat Brain Stem

Konstantin Hartmann and Michael Brecht

Transparent Methods

EXPERIMENTAL MODEL AND SUBJECT DETAILS

All animal procedures were performed in strict accordance with the Humboldt-University Animal Care Committee's regulations. Procedures were approved by the State Office for Health and Social Affairs committee in Berlin (Protocol No. G0279/18). Male Long-Evans rats were provided by Janvier Laboratories (Le Genest-Saint-Isle, France). Experiments were done on adult animals (age $\geqslant$ five weeks).

METHOD DETAILS

Surgery

Animals (n=13) were anesthetized using intraperitoneal injections of urethane (1.5g/kg bodyweight). The skin covering the skull was shaved and the animals head was fixed in a stereotactic frame. Body temperature was maintained at 36°C using a rectal probe and a homeothermic blanket (FHC, 1201 Main St., Bowdoin, ME, 04287 USA). Before incision, we applied local anaesthesia with lidocaine 2%. The head was brought to level by using Bregma and Lambda measures. Four fixation screws were placed in the frontal bone and a head post was fixed to the screws and the bone using dental cement. For the cooling experiments, a first 2 x 1.5 mm craniotomy was placed along the longitudinal axis above the PAG (periaqueductal gray), centered 6.5 mm posterior and 0.75 mm lateral to Bregma. A 1 megaohm tungsten microelectrode (MicroProbes, 18247-D Flower Hill Way, Gaithersburg, MD, 20879 USA) was inserted into the left PAG 6.5 mm posterior and 0.75 mm lateral of Bregma in a depth of 4-4.5 mm depth. Ultrasonic vocalizations triggered by 1 second long, 100 Hz stimulation confirmed the correct placement of the electrode in the PAG. To expose the brainstem for the cooling and stimulation experiments, a craniotomy exposed the cerebellum by removing the

occipital bone 8 mm posterior and 4 mm bilateral of Bregma completely until the atlas (first vertebrae). Following a durotomy, the cerebellum was carefully removed using a vacuum pump (N86, KNF Neuberger GmbH, Alter Weg 3, 79112 Freiburg) connected to a glass pipet. The position of the obex was identified visually by the narrowing and surfacing of the 4th ventricle.

Brainstem cooling

Local cooling was achieved by a custom-build, fluid cooled Peltier element. A 4 x 4 mm Peltier element was outfitted with matching gold plate and an attached gold pin (0.5 mm diameter) on one side. The other side was cooled using a custom heatsink with chilled water running through it (Supplementary Figure 7). The cooling effect was measured with three thermistors on the contralateral side of the brainstem and during each trial, visual control ensured that cooling indeed reached the brainstem. Using three thermistors at different distances to the cooling probe allowed us to calculate the cooling strength. When applying 0.8 V and 0.825 A, we achieved a drop of 6°C at a distance of 2 mm to the tip after 45 seconds of cooling. These settings were used for all experiments to achieve the same tissue cooling.

The gold pin was then pseudo-randomly placed on the brainstem in a grid pattern ranging from 4 mm anterior of obex to 3 mm posterior of obex and from the midline up to 4 mm lateral of obex (Figure 1C). The grid spacing was 1 mm and we covered as many brainstem locations as possible. The gold pin was placed on the surface of the brainstem to prevent irreversible damage to the tissue.

At each cooling location, we initiated 29 electrical stimulations of the PAG to trigger calls. Stimulation consisted of a 1 second, 100 Hz stimulation of 220 ± 94 µA followed

by a 5 second inter-stimulus-interval and was controlled using PatchMaster (HEKA, Ludwigshafen/Rhein, HRB 41752). After stimulation 7, the Peltier element was activated and kept cooling the brainstem until after stimulation number 17 when it was deactivated and the brainstem rewarmed itself. Vocalizations were recorded with a condenser ultrasound microphone CM 16/CMPA (Avisoft-Bioacoustics e.K., Schoenfliesser Str. 83, 16548 Glienicke/Nordbahn, Germany) attached to an Avisoft Bioacoustic UltraSoundGate 416H and recorded using the Avisoft-RECORDER software.

Microstimulation of the brainstem

For stimulation experiments the cerebellum was removed as described above. We positioned the electrode in the same grid as described for the cooling above. Each position was chosen in a pseudorandom order to account for the duration of the experiment. At each location, we electrically stimulated the brainstem in 500 µm depth-steps starting dorsally. Stimulation was controlled using Spike2 (Cambridge Electronic Design Limited, 139 Cambridge Road, Milton, Cambridge, England) For each location, we determined if vocalizations could be triggered with a maximum current of 200 µA. After a mapping was completed, we placed electrolytic lesions (DC currents, tip neg, 8 µA, 10 s) the brainstem sites, at which we evoked the most robust vocalizations at the lowest thresholds. Then the animal was overdosed with 8 ml urethane followed by a transcardial perfusion (phosphate buffer followed by a 4% paraformaldehyde solution) and removal of the brain for histological processing.

Histology

To recover the lesion of the electrical stimulation experiments, the brains were sliced and stained as follows. After perfusion, the brains were fixed for 12-24h in 4% PFA in the fridge. Thereafter, they were sliced with a vibratome.

For Nissl staining, mounted brain sections (100 µm) were washed 2 minutes each in 90, 80 and 60% of ethanol in descending order, followed by 1 minute in aquadest kresyl-violet (1% kresyl-violet in NA-acetate buffer with a pH between 3.8 and 4.0) staining was applied for 40-50 seconds and then rinsed with aquadest for 30 seconds. For differentiation, we used 80% ethanol and 10% acetic acid, followed by 10-20 seconds in 96% ethanol. Before coverslips were added, brain sections were dehydrated with Isopropanol for 2 minutes and twice xylol for 5 minutes each. Pictures were taken on an Olympus BX51 microscope.

Myelin staining was performed on free-floating sections that were incubated for 2-4 hours in a 0.1% solution of gold in 0.02 M PB, ph7.4, and 0.9% sodium chloride. After staining, sections were rinsed for 5 minutes, fixed for 5 minutes in a 2.5% solution of sodium thiosulfate, and rinsed for 30 minutes before mounting with Mowiol.

For NeuN staining, floating brain sections (60 µm) were washed in 0.1 M phosphate buffer saline (PBS), followed by twice washing in 0.1 M PBS + 0.5% Triton-X. Blocking was done with 2.5% BSA + 0.75% Triton-X in 0.1 M PBS for one hour. Brain sections were then stored in 1% BSA + 0.3% Triton-X with NeuN (rabbit) 1:1000 concentration for 3 days on a shaker at 4°C. After 3 days, brain sections were washed 3 times with 0.1 M PBS. For the second antibody, we used Anti-NeuN (DAR rabbit polyclonal Fluor® 488 Conjugate LOT:3209767 by Millipore) with 1:200 concentration. The antibody was applied for 24 hours with 1% BSA in 0.1 PBS. After 3 washings with 0.1 PBS brain sections were mounted with Fluoromount® (Biozol, Eching, Germany)

mounting medium. Pictures were taken on a Leica DM5500B and subsequently adjusted with brightness and contrast.

Analysis of cell size was done manually with imageJ (Abràmoff et al., 2004). For each region, we sampled 600 cells, 50 per brain section in two animals. Overlapping and out of focus cells were not measured. Analyzed PCRtA ranged from Bregma -10.0 to -10.3 mm. VoPaRt, sp5, IrtA ranged from -10.5 to -11.2 mm. PCRt from -11.6 to -13.5 mm. Amb from -12.2 to -13.5 mm. MdD, MdV, Irt, NRA from -14.3 to -15.5 mm (all measures relative to Bregma).

Quantification of myelinization was done with imageJ as well. Measures were taken bilaterally of three brain sections in three brains each, resulting in 18 measures. We used a rectangle spanning from the lateral boarder of sp5 to the midline of the brainstem. The upper box limit was adjusted to be at the boarder of solitary tract (Sol) and the lower boarder touching the facial nucleus. We took the gray value profile along the horizontal axis. We interpolated each measure to a uniform length and normalized the values relative to the maximum myelinization of each brain section, resulting in a value between 0 and 1, where 1 always represented the maximum myelinization in the trigeminal tract and 0 the lowest measured myelinization elsewhere. The resulting normalized measures where then averaged and smoothed with a gaussian smoothing window of 10.

QUANTIFICATION AND STATISTICAL ANALYSIS

Analysis of Vocalizations

General analysis of cooling effects on calls was conducted with the automatic call detection and analysis tools of Avisoft SASLab Pro (Avisoft-Bioacoustics e.K., Schoenfliesser Str. 83, 16548 Glienicke/Nordbahn, Germany). For each cooling location, we analyzed calls evoked by three stimulations during the warm period, as well as the three last stimulations during the cooling period. Threshold for detection was set to -20 dB attenuation, call elements with less than 50 ms of interruption were considered one call. Number of evoked calls, maximum amplitude and maximum duration of calls was measured. For further analysis, we calculated the z-scores of the change between warm and cooled calls ((# calls cold - # calls warm)/(# calls cold - # calls warm)). Results were presented as a 2D map of the brainstem. For illustration purposes and to account for possible alignment differences between animals, the maps were smoothed with a Gaussian distribution. For Gaussian smoothing, we first increased the data matrix 18-fold and then applied a smoothing kernel with a standard deviation of 7. We included the raw data in unsmoothed maps in the supplementary section.

Maps depicting the cooling effects on high vs low frequency effects were scored manually. The scoring of the audio files was done blind, meaning that the cooling location of each file was unknown to the scoring person. Scoring done with Audacity (iWeb Media Ltd., Malta). The experimenters scored if high or low frequencies were affected by cooling in a subjective but repeatable fashion. The limits of this analysis are obvious and have thus been addressed in a second, objective analysis described below. As a threshold to discriminate between high and low frequencies we chose 30 kHz. This is a clear division between low frequency, fear calls and high frequency, positive calls (Brudzynski, 2005; Knutson et al., 2002; Panksepp and Burgdorf, 2003; Schwarting et al., 2007).

To extend upon this qualitative analysis, we conducted a second, quantitative analysis for our three focal locations, identical to the quantitative analysis of general call characteristics described above. The focus on a subset of trials and regions was necessary, since only trials were a single PAG stimulation induced both high and low frequency calls could be included in this analysis, greatly reducing the number of available trials (n=18). The number of high (>30 kHz) and low frequency (<30 kHz) calls was counted for 3 trials before cooling and the last three trials of cooling, identical to the general analysis of call effects. Next, the z-score between warm and cold periods was calculated and the data was grouped based upon their recording location (VoPaRt, NRA or central) and their frequency (high or low).

Analysis of brainstem stimulation evoked calls was done in a straightforward fashion. For each location, it was noted if a call could be evoked and if it was above of below 30 kHz. Generation of maps was done identical to the cooling results. If calls showed elements of both above and below 30 kHz, we omitted them from the frequency specific analysis. For analysis of the slope of calls, DeepSqueak (Coffey et al., 2019) was used.

Statistical analysis

We used MATLAB 2019b (Mathworks) for the statistical analysis of our data.

To test if the three defined regions are distinctly different from each other, we used the nonparametric Friedman test for paired data. For statistical testing, we used the raw, unsmoothed data. To obtain the specific differences between regions, we applied the Tukey-Kramer *post-hoc* test. For the analysis of the slope of calls upon brainstem stimulation, we used the Wilcoxon rank-sum test since some stimulation sites in the

center region did not evoke calls and thus, we could not measure the slope of the calls sufficiently.

Shuffling test

Potentially, one could assume that the distribution of measures and the resulting maps are occur out of a random distribution of the measures. To test whether the defined regions stem from such a random distribution or are indeed different from it, we applied a random shuffling test. We randomized the location ID of each measurement 10000 times and then compared the random distribution against the measured values at the same location. This method kept the obtained data and the spatial layout of our experiments intact and allowed to test if the observed results is different from random.

Cross-correlation

Cross-correlation between cooling effects and evoked calls was done with the Pearson Correlation.

Anatomical data

Comparison of cell sizes was performed with the non-parametric Kruskal-Wallis test since the data was not normally distributed. *Post-hoc* analysis of the Kruskal-Wallis tests was done with the Tukey-Kramer test. Normal distributed, paired myelinization data was analyzed with the Friedman test and the Tukey-Kramer *post-hoc* test.
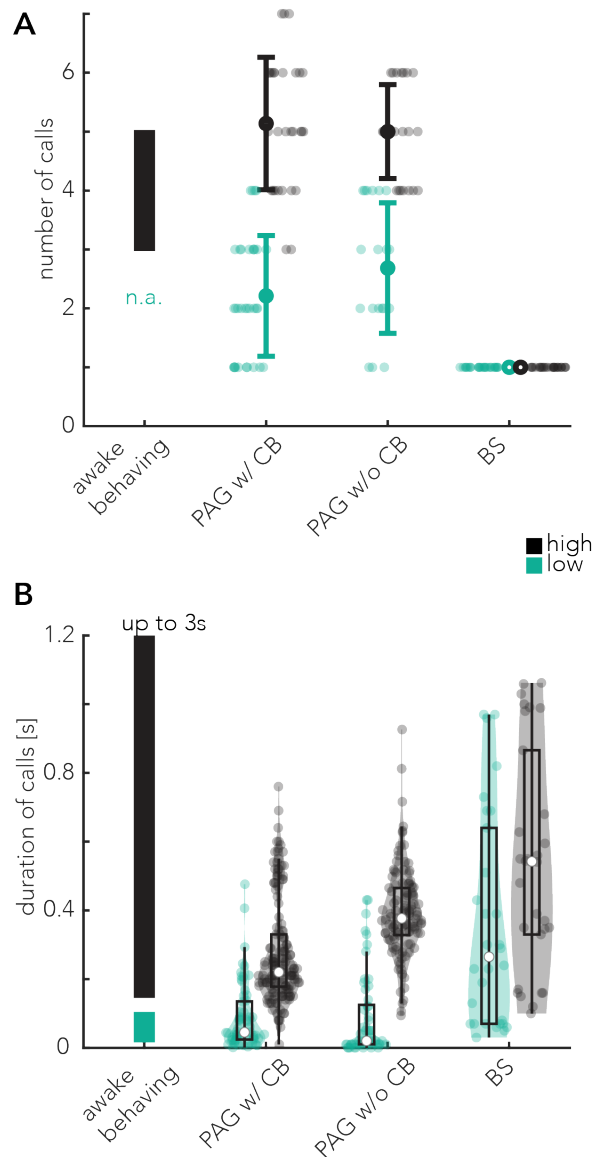
Supplementary Figure 1, related to Figure 1: Comparison between evoked calls under different animal conditions.

A) Mean number of evoked calls in awake behaving animals, upon PAG stimulation with and without cerebellum and direct brainstem stimulation. Solid bars in the awake behaving column are taken from literature (Schwarting and Wöhr, 2012). High frequency calls are not quantifiable since there are no clear single stimuli triggering them. Whiskers depict the standard error, dots show single data points.

B) Duration of high frequency and low frequency calls. The distribution of the violin plot shows the probability density of the cell sizes overlaid with boxplots. Solid bars in the awake behaving column are taken from literature. Awake behaving condition taken from literature (Ishiyama and Brecht, 2016; Schwarting and Wöhr, 2012).
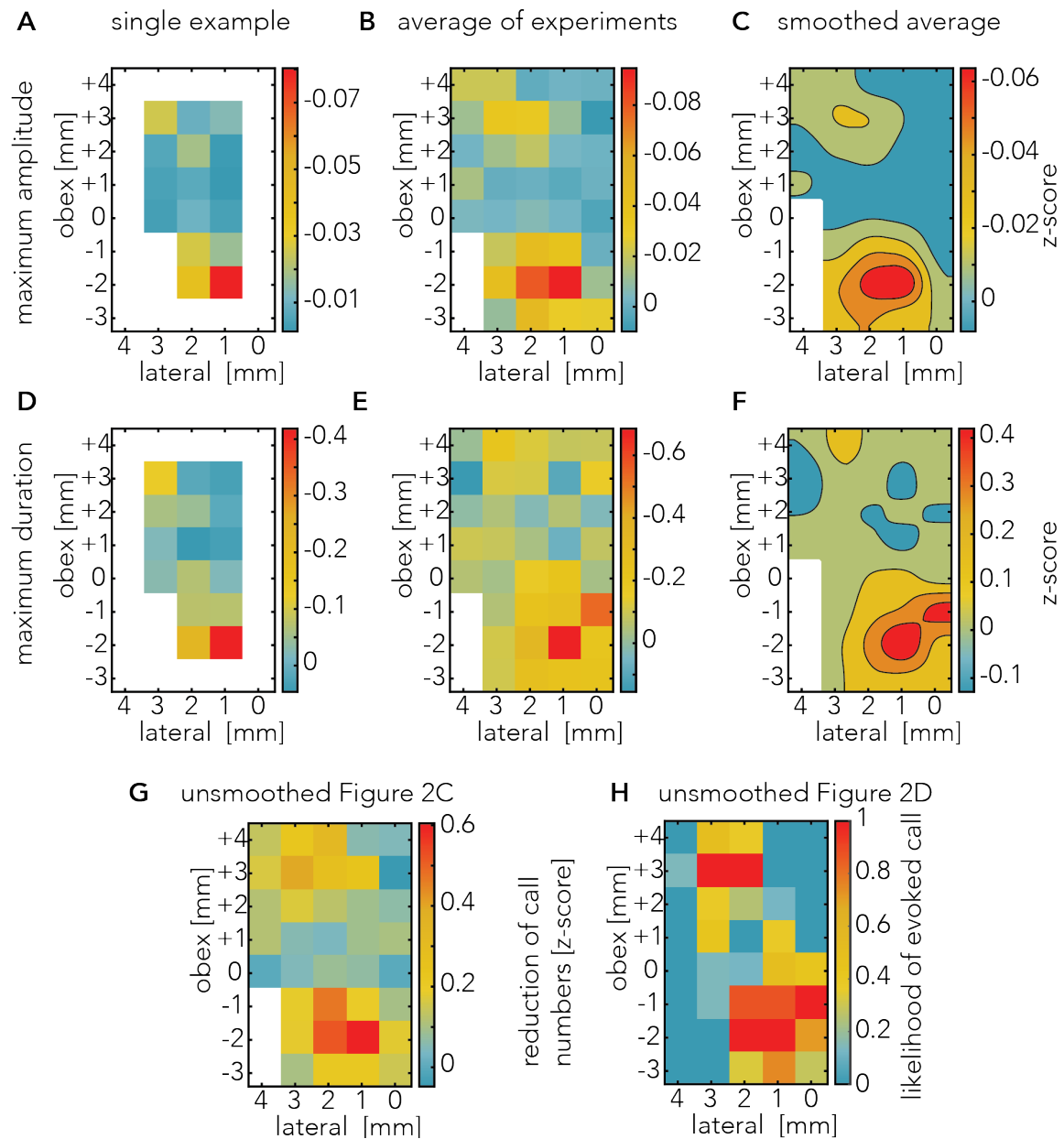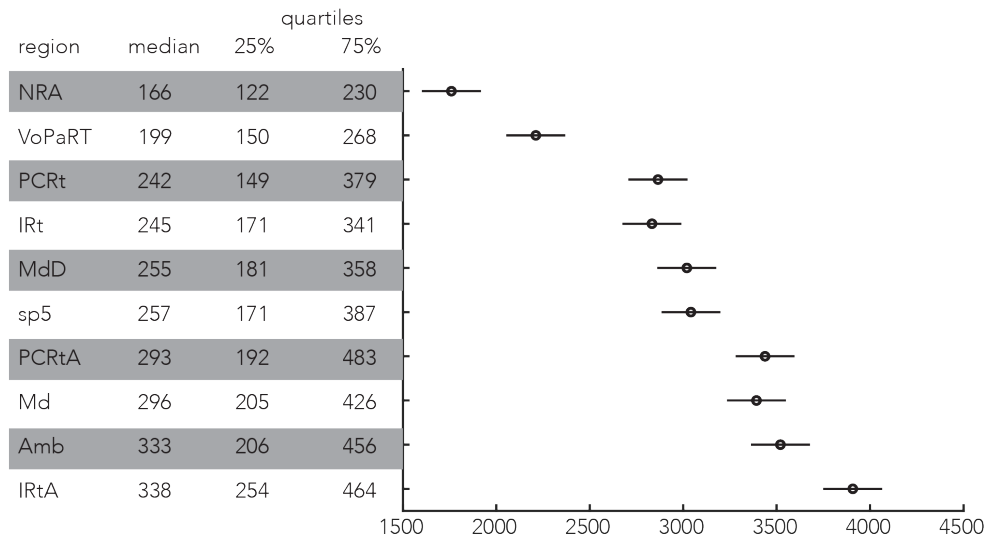
Supplementary Figure 2, related to Figure 2: Raw results of cooling and stimulation mapping experiments.

A-C) Maximum amplitude change after cooling, depicted as the z-score between cold and warm condition.

A) Single experiment, same as Figure 2A.

B) All experiments averaged, not smoothed.

C) Smoothed map of B.

D-F) Maximum duration of calls depicted as the z-score between cold and warm condition.

D) Single experiment, same as Figure 2A.

E) All experiments averaged, not smoothed.

F) Smoothed map of E.

G) Unsmoothed map of Figure 2C.

H) Unsmoothed map of Figure 2D.

A

region	median	quartiles 25%	75%
NRA	166	122	230
VoPaRT	199	150	268
PCRt	242	149	379
IRt	245	171	341
MdD	255	181	358
sp5	257	171	387
PCRtA	293	192	483
Md	296	205	426
Amb	333	206	456
IRtA	338	254	464

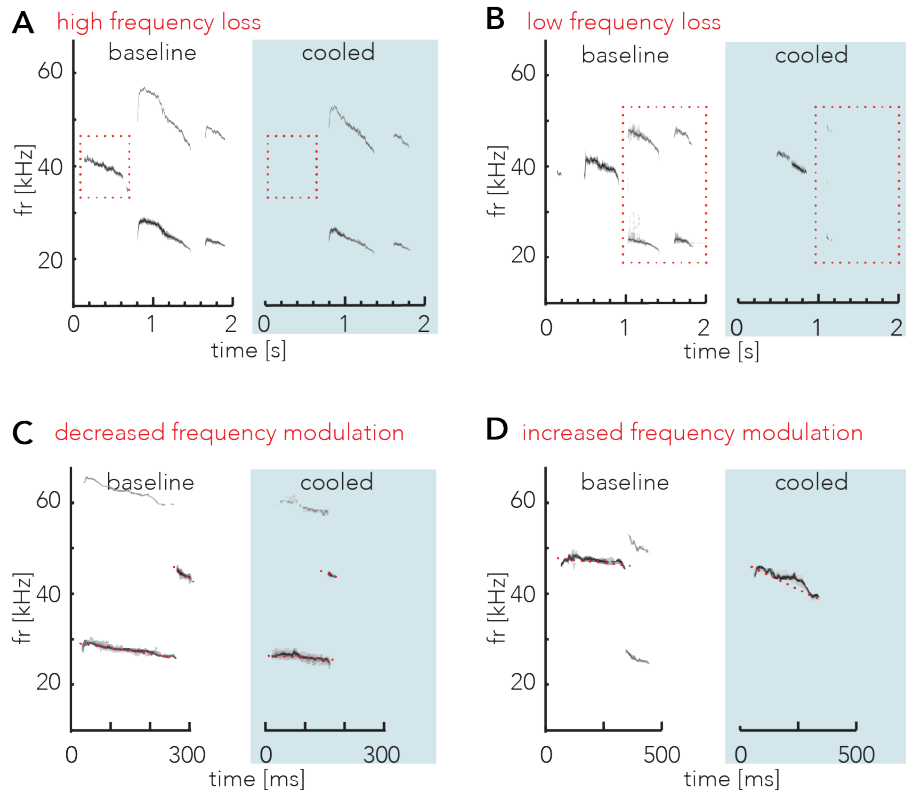**Supplementary Figure 3, related to Figure 4:**

A) Median cell cross sections in µm^2 as well as the lower and upper quartiles. The plot on the right is the result plot of the Tukey-Kramer with arbitrary units on the x-axis. If whiskers of two areas do not overlap, the difference is significant, see Table 1.
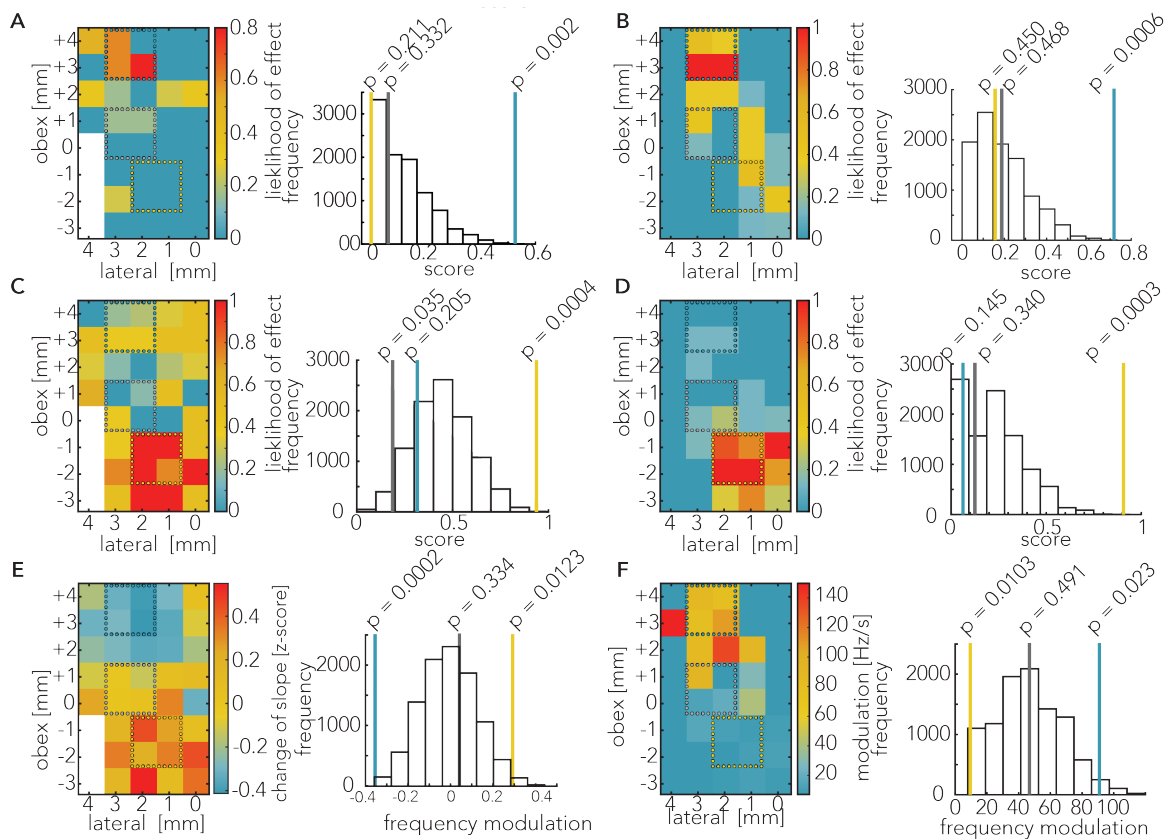
Supplementary Figure 4, related to Figure 5: Raw data for frequency and modulation specific effects and statistical analysis results.

A-F) On the left, the map shows the raw results of the cooling or stimulation results. On the right, the histogram shows the shuffled distribution of the results as well as the measured values of the target regions. Description of plots can be found along the description of the results shown in Figure 2 and 4.

A) Cooling effect on high frequency calls.

B) Stimulation evoked high frequency calls.

C) Cooling effect on low frequency calls.

D) Stimulation evoked low frequency calls.

E) Modulation (slope) of calls after cooling.

F) Modulation (slope) of stimulation evoked calls.

Supplementary Figure 5, related to Figure 5: Example cooling effects on high and low frequency calls and frequency modulation.

A) Second example of high frequency loss upon cooling of the brainstem in the VoPaRt.

B) Another example of low frequency loss upon cooling of the brainstem in the NRA region.

C) Decreased absolute frequency modulation when cooling the VoPaRt.

D) Increased absolute frequency modulation when cooling the NRA.
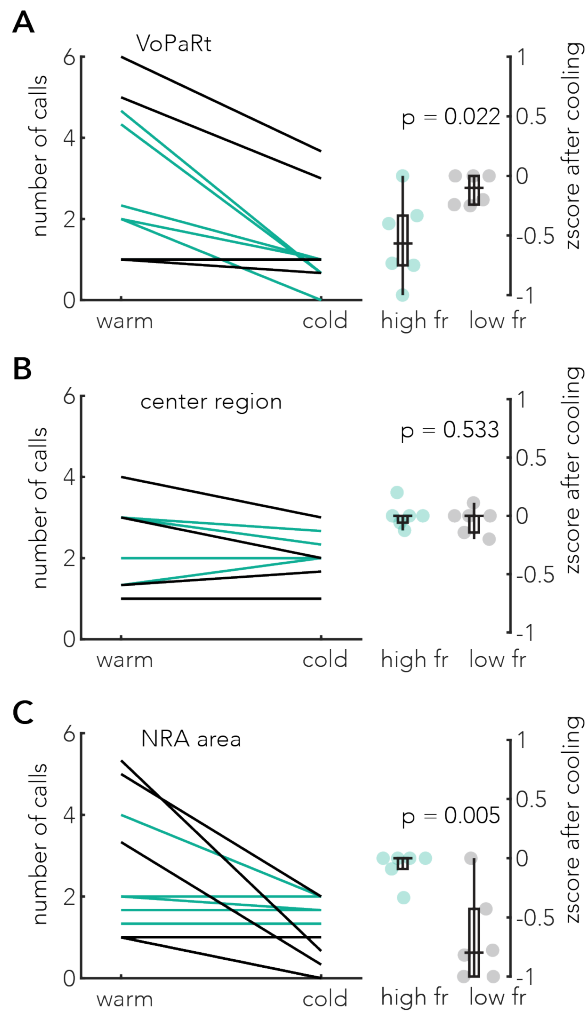
Supplementary Figure 6, related to Figure 5: Quantitative analysis of cooling of the VoPaRt region.

A) Black lines show the mean number of calls evoked by the last 3 trials before cooling and the mean number of calls evoked by the last 3 trials at the end of the cooling period. Cyan lines show the same results for the high frequency numbers (n=6 for each). The boxplot on the right side depicts the z-score for each frequency type after cooling.

B) Same as A, now for the central region.

C) Same as A and B, now for the NRA region.

tubing for water cooling of heat sink
power for peltier element
gold pin
perltier element
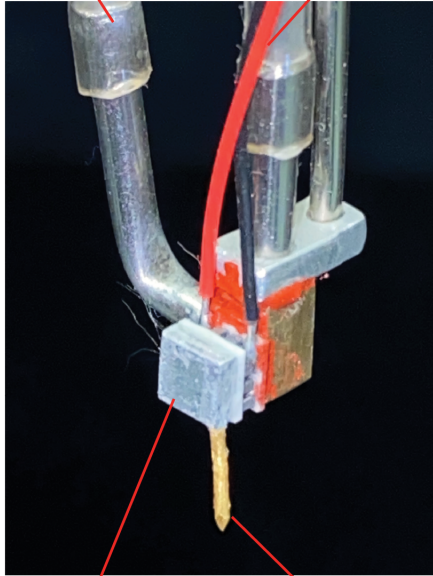
Supplementary Figure 7, related to Methods and Figure 1: Cooling element used in this study.

Supplementary Table 1, **related to Figure 4**: Statistical results of the Tukey-Kramer test of cell sizes. Third and fifths column show the lower and higher 95% confidence interval. Fourths column the difference between the group ranks and the sixth column the associated p-value.

Area 1	Area 2	lower 95%	Group diff.	upper 95%	p-value
NRA	VoPaRt	-768.0287	-451.66022	-135.29174	0.0002692
NRA	PCRt	-1421.5537	-1105.1852	-788.81674	0.0000001
NRA	IRt	-1389.5204	-1073.02	-756.51965	0.0000001
NRA	MdD	-1576.1004	-1259.7319	-943.36341	0.0000001
NRA	sp5	-1597.882	-1281.5136	-965.14508	0.0000001
NRA	PCRtA	-1994.567	-1678.1986	-1361.8301	0.0000001
NRA	MdV	-1948.4954	-1632.1269	-1315.7584	0.0000001
NRA	Amb	-2077.078	-1760.5776	-1444.0772	0.0000001
NRA	IRtA	-2464.2254	-2147.8569	-1831.4884	0.0000001
VoPaRt	PCRt	-969.76152	-653.525	-337.28848	0.0000001
VoPaRt	IRt	-937.72829	-621.35981	-304.99133	0.0000001
VoPaRt	MdD	-1124.3082	-808.07167	-491.83514	0.0000001
VoPaRt	sp5	-1146.0899	-829.85333	-513.61681	0.0000001
VoPaRt	PCRtA	-1542.7749	-1226.5383	-910.30181	0.0000001
VoPaRt	MdV	-1496.7032	-1180.4667	-864.23014	0.0000001
VoPaRt	Amb	-1625.2859	-1308.9174	-992.54892	0.0000001
VoPaRt	IRtA	-2012.4332	-1696.1967	-1379.9601	0.0000001
PCRt	IRt	-284.20329	32.1651906	348.533671	0.9999994
PCRt	MdD	-470.78319	-154.54667	161.689856	0.8734727
PCRt	sp5	-492.56486	-176.32833	139.90819	0.7580039

PCRt	PCRtA	-889.24986	-573.01333	-256.77681	0.0000006
PCRt	MdV	-843.17819	-526.94167	-210.70514	0.0000061
PCRt	Amb	-971.76089	-655.39241	-339.02392	0.0000001
PCRt	IRtA	-1358.9082	-1042.6717	-726.43514	0.0000001
IRt	MdD	-503.08034	-186.71186	129.656623	0.6915050
IRt	sp5	-524.862	-208.49352	107.874957	0.5382060
IRt	PCRtA	-921.547	-605.17852	-288.81004	0.0000002
IRt	MdV	-875.47534	-559.10686	-242.73838	0.0000011
IRt	Amb	-1004.058	-687.5576	-371.05721	0.0000001
IRt	IRtA	-1391.2053	-1074.8369	-758.46838	0.0000001
MdD	sp5	-338.01819	-21.781667	294.454856	1.0000000
MdD	PCRtA	-734.70319	-418.46667	-102.23014	0.0011742
MdD	MdV	-688.63152	-372.395	-56.158477	0.0074643
MdD	Amb	-817.21422	-500.84574	-184.47726	0.0000242
MdD	IRtA	-1204.3615	-888.125	-571.88848	0.0000001
sp5	PCRtA	-712.92152	-396.685	-80.448477	0.0029033
sp5	MdV	-666.84986	-350.61333	-34.37681	0.0163780
sp5	Amb	-795.43255	-479.06407	-162.69559	0.0000725
sp5	IRtA	-1182.5799	-866.34333	-550.10681	0.0000001
PCRtA	MdV	-270.16486	46.0716667	362.30819	0.9999858
PCRtA	Amb	-398.74755	-82.379072	233.989408	0.9982393
PCRtA	IRtA	-785.89486	-469.65833	-153.42181	0.0001137
MdV	Amb	-444.81922	-128.45074	187.917742	0.9573058
MdV	IRtA	-831.96652	-515.73	-199.49348	0.0000110
Amb	IRtA	-703.64774	-387.27926	-70.910781	0.0042466